Journal of Materials Chemistry A

Accepted Manuscript

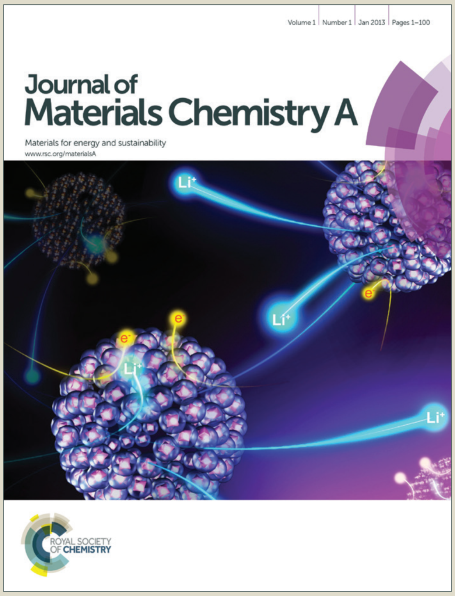

ROYAL SOCIETY
OF CHEMISTRY

www.rsc.org/materialsA

Cite this: DOI: 10.1039/c0xx00000x

www.rsc.org/xxxxxx

ARTICLE TYPE

Ag-encapsulated Au plasmonic nanorods for enhanced Dye-Sensitized Solar Cell performance

Hua Dong,[a] Zhaoxin Wu,*[a] Ahmed El-Shafei,[b] Bin Xia,[a] Jun Xi,[a] Shuya Ning,[a] Bo Jiao,[a] and Xun Hou[a]

Received (in XXX, XXX) Xth XXXXXXXXX 20XX, Accepted Xth XXXXXXXXX 20XX
DOI: 10.1039/b000000x

In this article, the Ag-encapsulated Au nanorods (Au@Ag NRs) are prepared and introduced into dye-sensitized solar cells (DSSCs). As a unique plasmonic nanostructure, this composite exhibit the superiorities on enhancing light-harvesting as well as restraining charge recombination of DSSCs. Remarkably enhanced light absorption of photoanode can be obtained via the Surface Plasmon Resonance (SPR) effect of the Au@Ag NRs, meanwhile a broadened absorption in the red and near-infrared (NIR) region ensures the full utilization of the solar energy. Beyond the dominated optical utility, the presence of the Au@Ag NRs promotes the suppression of the charge recombination, further enhancing the photochemical catalysis of DSSCs. The optimized Au@Ag NR modified DSSC is achieved with the power conversion efficiency of 8.43%, which is significantly superior to that of the pure TiO_2 DSSC with the PCE of 5.91%.

1. Introduction

Recently, Dye-sensitized solar cells (DSSCs) have attracted significant attention and reach up to 13 % power conversion efficiency.[1, 2] Due to its easy fabrication, low cost and high photon-to-electric power conversion efficiency, this type of cell has been expected as a potential alternative to conventional silicon-based solar cells.[3, 4] Extending the response of dye sensitizers to a broader range of the solar spectrum and improving the light-harvesting efficiency (LHE) of the photoanode are the critical factors to improve the performance of the DSSCs.[5] Therefore, to obtain a higher efficiency, considerable efforts on the dye-adsorbed photoanode have been explored, which mainly focused on the design of new dye molecules and the structure-modified technology of the photoanode films.

Over 90% energy of the sunlight was concentrated in visible and near-infrared (NIR) region,[6] so a high-efficiency sensitizer applied in DSSCs was expected to exhibit a wide absorption spectrum. Today, the most universal sensitizers, such as N3, N719 and C106,[7] could only make effective use of the sunlight at the region of 400 nm to 650 nm. The rather low utilization of red and NIR region limit the light harvesting efficiency at longer wavelength, which seem to be a bottleneck of the device efficiency. Recently, new sensitizers were designed to extend the absorption to red or NIR region.[8-10] However, the overall efficiency was not improved cause the decreased availability of the new dyes at the short wavelength. Co-sensitized technology was another approach to fully utilize the energy of the sunlight,[11, 12] whereas the complexity of the fabrication process and the match of the energy level at sensitizer/semiconductor interface remains unsolved perfectly. As the consequence, keeping the strong absorption at visible region as well as increasing the harvesting at longer wavelength is the most suitable development tendency.

Based on the conventional sensitizers, Surface Plasmon Resonance (SPR) effect was employed as an attractive approach higher light harvesting efficiency recently.[13, 14] Plasmonic metal-nanoparticles such as Ag nanoparticles, Au nanoparticles, and core-shell nanostructures could boot the performance of DSSCs via SPR effect.[15-22] SPR is collective oscillation of conduction band electrons in a metal nanoparticle driven by the electromagnetic field of incident light, which could significantly increase the light absorption of the dye and the generation of the photon-carriers. However, the absorption spectrum of reported plasmonic particles is located in short wavelength of the visible light. Actually, reported plasmonic applications could only enhance the LHE to some extent, and the limitation is that the improvement of LHE was just presented at the relatively narrow range.[23, 24]

To achieve a win-win course of both enhancing the response of sensitizers and extending the light harvesting region of the photoanode, preferable choice is developing the novel plasmonic nanocomposites with the extensive absorption spectra. In this article, a unique (Au core)−(Ag shell) nanorods (Au@Ag NRs) was explored and applied in the photoanode of DSSCs， as shown schematically in **Fig. 1**. "Rod-like" metal nanostructures have the tunable longitudinal and transverse plasmon absorption from visible to the NIR region, which could provide a unique opportunity for utilizing the low energy range of the solar energy.[25] The coupling effect between Ag and Au exhibit much stronger electric field enhancements than pure Au nanostructures, which achieved a rather wide plasmonic wavelength from 350~900 nm with four strong SPR peaks. With the introduction of the Au@Ag NRs, both the increased absorption of dye and broadened absorption region of the photoanode were achieved. In addition to the primarily contributions on LHE, the Au@Ag NRs present the capability on the suppression of the charge recombination, which could further improve the performance of the DSSCs. Considering the stability and easy-modified process, the prospect of this type nanorods is brilliant in future.

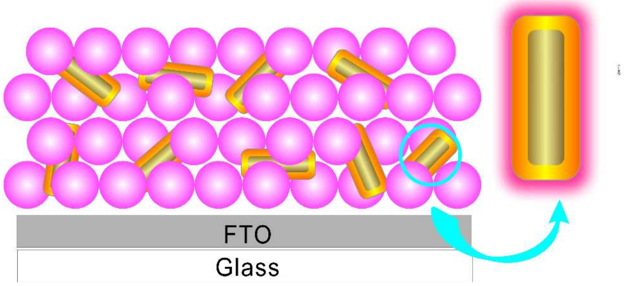

Fig. 1 Schematic structure of DSSCs with Au@Ag NRs in a TiO_2 film incorporated

2. Results and discussion

2.1. Properties of the bristled Au@Ag NRs

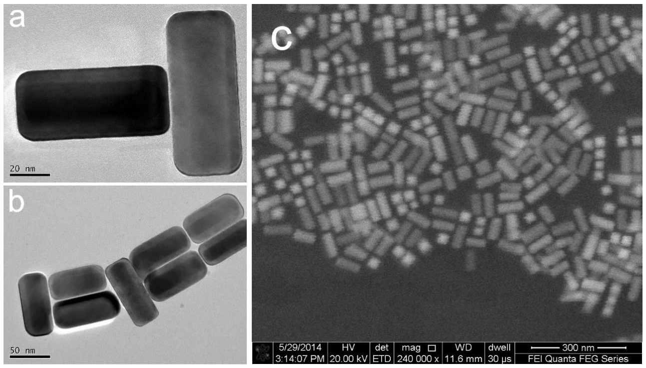

Fig. 2 TEM images of the Au@Ag NRs (a,b) and SEM image of the Au@Ag NRs (c).

Fig. 2a and b show the TEM images of the Au@Ag NRs, and **Fig. 2**c shows the SEM images of the Au@Ag NRs. It can be seen that the Au@Ag NRs have narrow shape and size distributions. The average length and diameter of Au core are 65 ± 4 nm and 15 ± 2 nm, and the two parameters of Ag shell are 70 ± 5 nm and 28 ± 3 nm. The EDX spectrum was used to analyze the ingredient of the Au@Ag NRs, and the Ag, Au peaks were observed clearly. (shown in **Fig. S1**†)

The preparation of elongated anisotropic Ag nanostructures with uniform shape and narrow size distributions has been proven challenging.[26] Au nanorods, due to the attractive advantages, such as facile growth process, tunable-longitudinal plasmon wavelengths, and chemical stability, could function as excellent supports for the formation of Ag shells.[27] The synthetic (Au core)−(Ag shell) nanorods were expected to exhibit specific plasmonic bands determined by the coupling effect between Ag and Au. Meanwhile, the plasmon wavelengths range can be tailored in the visible to near-infrared regions by varying the Au core size and the Ag shell thickness.[28, 29]

Appropriate plasmonic wavelength of the nanorods is the premise applied in DSSCs. The absorption peak of metal nanostructures, that is, the plasmon band, is dependent on the shape and ratio.[30] In our experiments, this “rod-like” Au@Ag NR has the longitudinal and the transverse plasmon absorption.

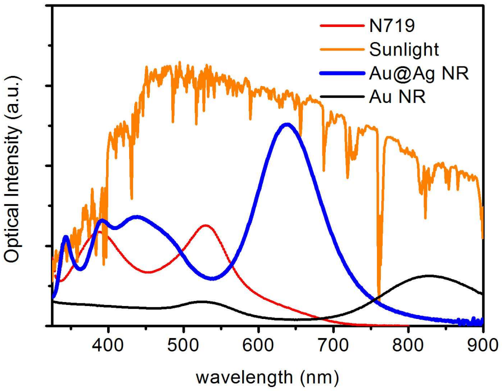

Fig. 3 Solar irradiance spectrum of ASTM G173-03 reference (AM 1.5) and absorption spectrum of the Au@Ag NRs and N719.

As is shown in **Fig. 3**, there are four strong plasmon resonance peaks regarded as the optical signatures of Au@Ag NRs. To clarify the evolution of surface plasmon bands after growth of Ag shell compared with Au nanorod, the absorption spectrum initial pure Au NRs (average length and diameter are 65 ± 4 nm and 15 ± 2 nm) was also measured. The longitudinal and transverse plasmon resonance wavelengths of the initial Au nanorod sample dispersed in aqueous solutions are 828 and 521 nm, respectively. After coating the Ag shell with appropriate thickness, the two plasmon peaks blue-shift to 640 and 437 nm, respectively.

Referring to the previous report, since the plasmon resonance wavelength of Ag nanstructures is generally shorter than that of Au nanostructures with the same shape and size, the blue shift of longitudinal surface plasmon wavelength (828 nm to 640 nm) can be understood as arising from both the reduction in the aspect ratio of the Au@Ag nanorods and the effect of the optical properties of Ag shell over Au core. The blue shift of the transverse surface plasmon wavelength (521nm to 437 nm) can be attributed to the coating of silver, cause the Ag shell is thick enough to screen the Au on the transverse aspect.

The two emerging wavelength (343 nm and 390 nm) are indicative of the surface plasmon mode of Ag. Two peaks appeared after the Ag shell reached a certain thichness, and they only red-shift very slightly as the Ag shell was further increased.[25] So the characteristic of the Au@Ag NRs is the tunable longitudinal and transverse plasmon resonance wavelengths of the initial Au NRs. The multiple plasmonic peaks of the nanorods promised an extensive visible-to-NIR coverage.

In addition to the wide absorption feature of the nanorods, another unique characteristic of the metal nanocomposite, coupling effect between Ag and Au, could enhanced the electromagnetic field much larger than single metal nanostructures.[31] To further confirm the enhanced local field of the Au@Ag NRs, models of Au nanoparticles sphere (diameter =45 nm) and Au nanorod (same dimention as Au@Ag NRs) were built. A theoretical investigation on spatial properties of light trapping by SPR effect is developed to describe the speciality. Finite Difference Time Domain method (FDTD) is applied to calculate the LSP field distribution.

Fig. 4 shows the finite-difference time-domain (FDTD) simulation results of the field intensity enhancements of the

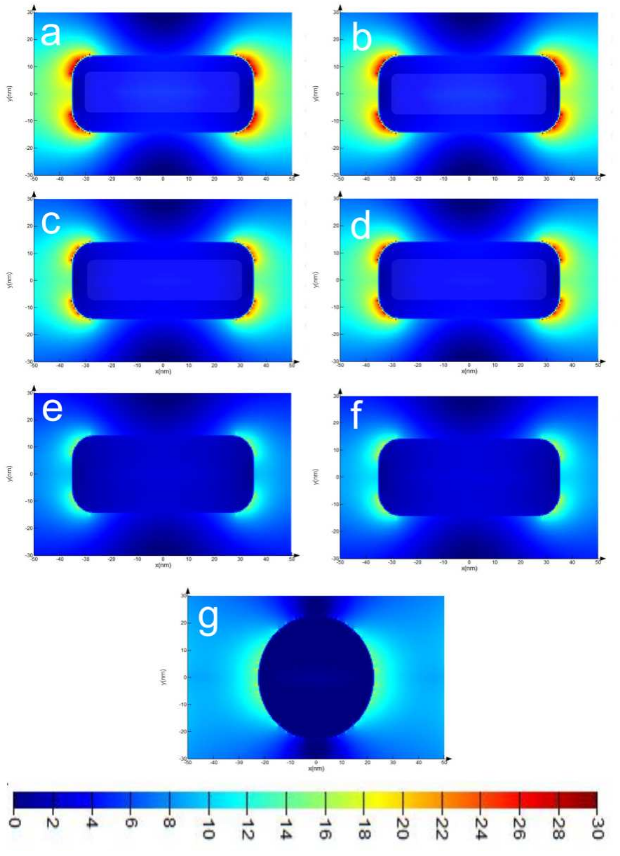

Fig. 4 The calculated distribution of localized electric field intensity around metal nanostructures at plasmon wavelengths: Au@Ag NRs (a) 343 nm (b) 390 nm (c) 437 nm and (d) 640 nm; Ag NRs (e) 530 nm (f) 651 nm; Ag NPs (g) 535 nm.

Au@Ag NRs, Au NRs and Au NPs. The field intensity enhancements were calculated under the excitation at their plasmon wavelengths. It was found that the electrical field intensity of the Au@Ag NRs obviously enhanced compared with the pure Au NRs and Au NPs. The field intensity enhancement factors along the central length axis are plotted in **Fig. 5**. The enhancement factors of the Au@Ag NRs are 3.1−5.2 times those of the Au nanorod (at 651nm), and 4.0−6.8 times those of the Au nanoparticles. This is due to the fact that Ag nanocrystals exhibit much stronger electric field enhancements than Au nanocrystals,[25] and the coupling effect between Ag and Au also contributed to the higher factors. The simulation confirmed the unique local field enhancement effect of the Au@Ag NRs, which plays the role of research foundation in plasmonic enhanced DSSCs.

As is shown in **Fig. 3,** a considerable overlap between the absorption of N719 and the Au@Ag NRs guaranteed an effectively interaction, enhancing the photocatalysis property of the sensitizers. Moreover, the strong absorption of the Au@Ag NRs at the longer wavelength further promoted the sunlight harvesting at red and NIR region.

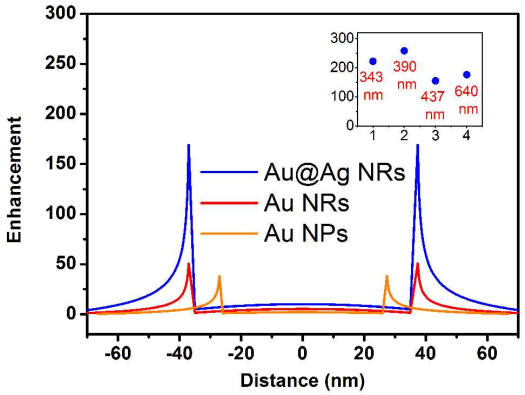

Fig. 5 Electric field intensity enhancement profiles along the length axis and passing through the center of the various metal nanostructures.

2.2. Stability and Absorption Spectroscopy

Referring to the plasmonic nanostructures applied in DSSCs, the chemical and thermal stability of the structure is very important. Bare metal nanoparticles could be easily corroded by electrolyte, and the thermal deformation will occur after the preparation of photoanode.[21] Considering this, protective layer around the nanorods is needed before incorporating the nanostructures into DSSCs. In our study, hydrolysis of titanium precursors was used for the formation of the thin TiO_2 shell around the nanorods.[15] **Fig. S2†** shows the TEM image and **Fig. S3†**a shows the EDX of the TiO_2 shell coated nanorods. As can be seen that, the TiO_2 shell coated on the nanorods is very thin (3~4 nm), which is beneficial for readily forming photoanode film with TiO_2 nanoparticles as well as reducing the corrosion and recombination. As the size and absorption properties of the processed nanorods were almost unchanged (shown in **Fig. S3†** b), previous discussion of the nanorods were still tenable. Up to this point, the application of the nanorods in DSSSs was realizable and meaningful.

A simple experiment has been developed to evaluate the corrosion resistance of the nanorods to the electrolyte. Same dose of electrolyte was added into bare Au@Ag NR colloidal solution and treated Au@Ag NR colloidal solution， and appearance variation was recorded for a period of time. As is shown in **Fig. S4†**, the color of bare Au@Ag NR colloidal solution become light and transparent eventually, and we speculated that bare nanorods were easily corroded by iodide/triiodide redox couple. By contrast，treated Au@Ag NR colloidal solution maintain a stable state all along, which confirmed the excellent chemical stability of the treated nanorods.

In order to assess the effect of the Au@Ag NRs on the light absorption of photoanodes, mesoporous TiO_2 films with different amounts of Au@Ag NRs incorporated were prepared (0.00wt%, 1.28wt%, 2.49 wt %, 3.68 wt %, 4.97 wt %). The SEM of surface morphologies of the various films were shown in **Fig. S5†**. As the amount of the Au@Ag NRs is rather low, all films showed compact morphologies and smooth surfaces with little difference. In addition, the ratio and the size of Au@Ag NRs exhibit no obvious deformation due to presence of the TiO_2 protecting layer.

Actually, there are two aspects influenced on the thermostability of the nanorods. Firstly, the thin TiO_2 shell coated on the nanorods served as the initial protecting layer; secondly, after mixing the nanorods with TiO_2 paste uniformly, the neighbouring TiO_2 nanoparticles around the NRs could provide effective insulation effect. Related literatures also reported the feasibility of the typical metal nanostructures with thin shell developed in DSSCs.[32, 33] This result demonstrates the good thermostability of the nanorods, and the multiple SPR features of the Au@Ag NRs could still play the role in DSSCs.

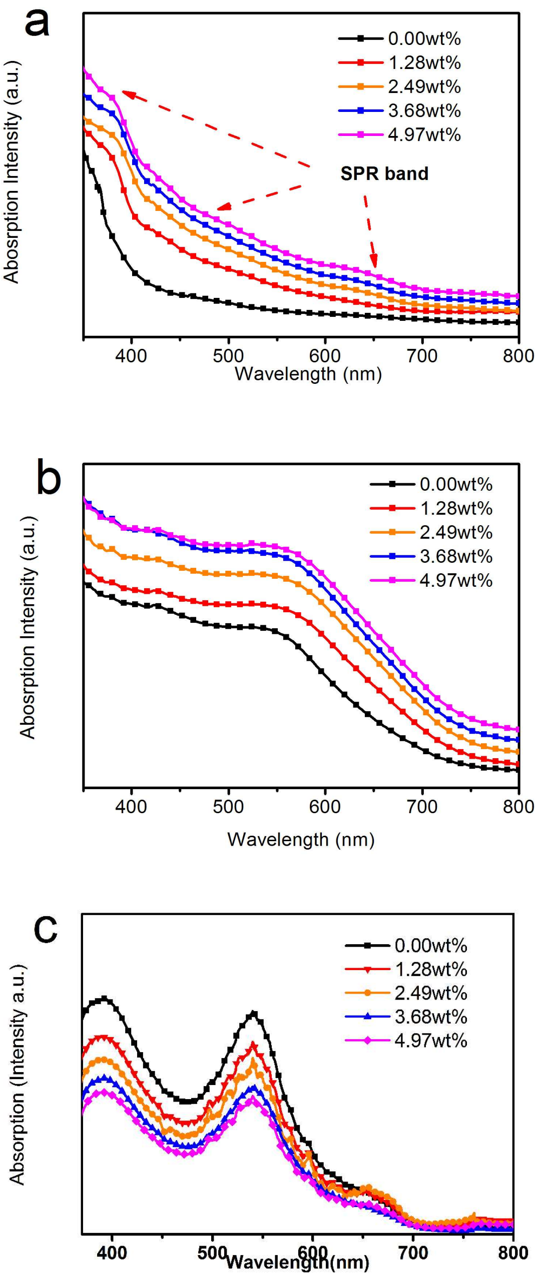

Fig. 6 (a) Absorption spectra of photoanodes with different concentration of Au@Ag NRs (b) Absorption spectrum of the different photoanodes absorbed dyes. (c) Absorption spectra of the desorbed N719 from dye-loaded TiO_2 film in NaOH solution.

UV-Vis absorption spectrums of the dye absence/adsorbed/de-sorption photoanode films were investigated and discussed in detail. **Fig. 6**a shows the dye-absence spectrums of various films, and observable SPR band appeared in the absorption spectrums of Au@Ag NRs incorporated TiO_2 films. The dye-adsorbed spectrums, shown in **Fig. 6**b, indicated that enhanced absorption of Au@Ag NRs incorporated TiO_2 films could performance on the whole visible and NIR region. The higher concentration of the Au@Ag NRs, the stronger intensity of absorption was obtained. The significantly enhanced and broadened absorption is mainly attributed to the SPR effect of the Au@Ag NRs. To confirm the inference, absorption spectra of the dyes **N719** desorbed from various films measured in NaOH solution were measured and shown in **Fig. 6**c. It was found that the intensity of absorption peak is slightly lowered with the presence of Au@Ag NRs, which clarified that the amount of the dyes in Au@Ag NRs incorporated films was less than that of pure TiO_2 film. This series of discussion strong supported for the views that the enhancement of the absorption is not due to the increase in the amount of dye but the SPR effect. The enhanced electromagnetic field around the Au@Ag NRs improved the interaction with the dye molecules dipoles and thus results in the enhanced light absorption of the dye and more charge carrier generation.[19, 21] Furthermore, a noticeable phenomenon, that is, a broadened spectra absorption range which extend to the red and NIR was observed. Based on the unique plasmonic properties of the Au@Ag NRs, enhanced dye absorption and broadened spectrum-absorption range of the photoanodes can be achieved for improving the performance of the DSSCs.

It was noted that when the concentration of the Au@Ag NRs was over 3.68%, the absorption intensity of dye-adsorbed films has almost no increased. Meanwhile, the amount of dye decreased due to the lower surface area of the film. With the increase of the Au@Ag NRs concentration, the SPR effect of the Au@Ag NRs enhanced at the expense of the lower absorbed dye amounts, so there is a suitable concentration for keeping the balance of the two aspects. Only then, the ability of the nanorods can be full played to boost the J_{sc} and the power conversion efficiency of DSSCs.

Here to further demonstrate the superiority and uniqueness of the Au@Ag NRs, pure Au NRs and Au nanoparticles with same dimension were prepared and applied in DSSCs. The TEM images of Au NPs and Au NRs with TiO_2 shell were shown as **Fig. S6†**. And the absorption spectra of three nanostructures with same particle number concentration were shown as **Fig. S7†**. Considering the academic rigour, the particle number concentration of the three nanostructures should be consistent for comparison. The density ratio of single Au@Ag NRs, pure Au NRs and Au nanoparticles was equal to 1:1.48:1.29. So 3.68 % Au@Ag NRs, 5.44 % Au NRs, and 4.74% Au NPs were applied into DSSCs.

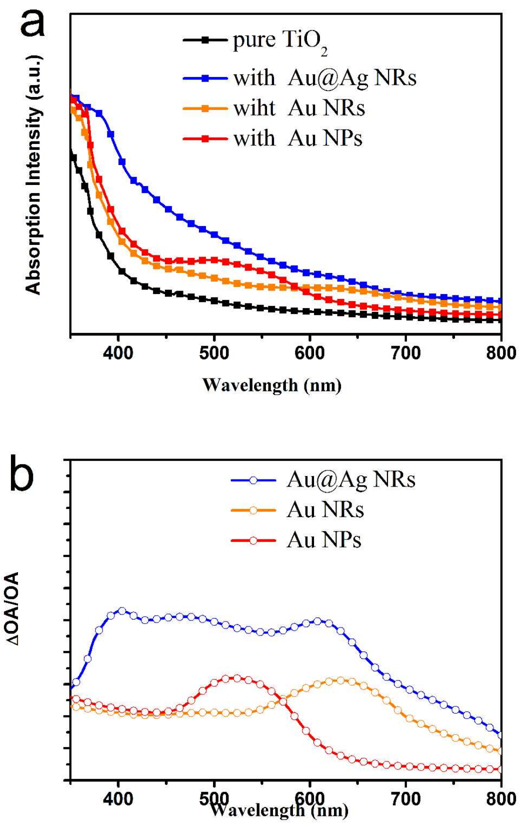

Fig. 7 UV-Vis absorption spectra of different photoanode films (a) and Relative changes in optical absorption (**ΔOA/OA**) of different photoanode films (b).

Fig. 7a show the absorption of photoanodes with and without three nanostructures at same particle number concentration, and it was found that enhanced absorption appeared in all nanostructures incorporated film. Pure Au NRs and Au NPs have the similar performance, and Au@Ag NRs was the optimal one.

To further study the enhanced mechanism, the relative changes in optical absorption (**ΔOA/OA**) of the various dye-absence photoanodes are shown in **Fig. 7**b.

Here the **ΔOA/OA** was defined as:

ΔOA/OA = (Abs (photoanode with nanostructure) – Abs (pure photoanode)) / Abs (pure photoanode)

As to the pure Au NRs and Au NPs, The relatively enhancement can be observed, and the enhancement band was coincide with the LSPR band position of single nanoparticles, respectively (**Fig. 7**b). It is noted that the performance of the Au@Ag NRs was distinctive. The **ΔOA/OA** of Au@Ag NRs was significantly broadened and enhanced compared to pure Au nanostructures, and enhancement band in the range of 350 nm-800 nm with three band (405 nm, 462 nm, 635 nm) is roughly accord with the plasmonic features of the single Au@Ag NRs. The results clarified that the coupling effect between Ag and Au could provide the capability of achieving strong localized field as well as extending the absorption to the red and NIR region. This advantage promoted the absorption of photoanode effectively compared with traditional metal nanostructures.

2.3. Photovoltaic Performance of DSSCs

To investigate the properties of Au@Ag NRs on the performance of DSSCs, the photocurrent–voltage (I–V) and incident photon-to-current conversion efficiency (IPCE) characteristics of DSSCs with different TiO_2 photoanodes were discussed and shown in **Fig. 8**a and b**,** and the performance parameters were summarized in **Table 1**.

It was found that the photocurrent has an obvious increase tendency with the concentration of Au@Ag NRs. The optimized J_{sc} of 16.53 mA cm^{-2} and PCE of 8.43% were achieved in the DSSC with the content of 3.68 wt%, which exhibit a 40% enhancement of PCE in comparison with that in the DSSC with pure TiO_2 photoanode. The enhancement of J_{sc} can be mainly attributed to the improvement of light harvesting efficiency in the visible and NIR region by plasmon-enhanced excitation. As the plasmonic wavelength of Au@Ag NRs has a considerable overlap with the strong energy of the sunlight, the effective SPR effect can be ensured. Owing to the coupling effect, remarkably enhanced localized electromagnetic field can be obtained. Then dye molecules around the neighbouring Au@Ag NRs could absorb more photons and convert the photons to charge carriers.

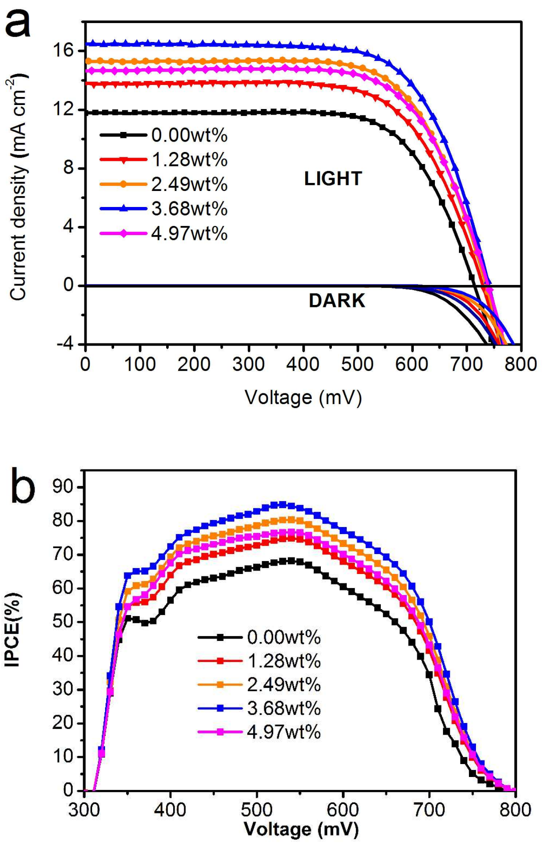

Fig. 8 (a) I-V and (b) IPCE characteristic of DSSCs with various TiO_2 photoanodes.

Another factor influenced on the J_{sc} was charge transport-recombination effect of the Au@Ag NRs. The apparent and uniform Fermi level of the metal nanostructure/TiO_2 interface could form electron-hole separation centers,[34] and this steady state of semiconductor-metal nanostructure contact could accelerate the movement of photo-generated electrons transporting from excited dye to TiO_2 nanoparticles, then it reduces the recombination of carriers and increased the J_{sc}.[35]

The dark-current reflects the recombination of charges in the conduction band of TiO_2 with triiodide to some extent. **Fig. 8**a shows the dark-current curves of different DSSCs. Compared to the DSSCs based on the pure TiO_2 film, the dark current of the DSSCs with Au@Ag NRs significantly decreased, which can be attributed to the suppression of the recombination between triiodide and electrons in the TiO_2 network.

Table 1 Photovoltaic characteristics of DSSCs with various TiO_2 photoanodes

group	V_{oc} (mV)	J_{sc} (mA cm^{-2})	FF	η (%)	R_{ct} (Ω)
Pure TiO_2	711	11.69	0.704	5.91	50.21
1.28%-Au@Ag NRs	728	13.74	0.698	6.88	54.34
2.49%-Au@Ag NRs	730	15.31	0.699	7.78	61.67
3.68%-Au@Ag NRs	729	16.53	0.701	8.43	67.50
4.97%-Au@Ag NRs	727	14.56	0.705	7.50	57.07

After reaching the maximum value at 3.68 wt%, the J_{sc} and PCE of the devices decreased along with the increase of the concentration of Au@Ag NRs. As the light absorption efficiency almost unchanged over 3.68 wt%, the change of J_{sc} was probably associated with the role of the electrical. Though the introduction of the nanorods was conductive to the suppression of the charge recombination for DSSCs, excess concentration of nanorods probably induced the flaw and the aggregation of TiO_2 film (shown in **Fig. S5**†). Then the capability of reducing recombination was weaken. The advantage of the increased light harvesting effect is offset by the recombination. And the dark current curves show the same tendency with the J_{sc}, further indicating the charge recombination influenced by the Au@Ag NRs.

The incident photon-to-electron conversion efficiency (IPCE) of DSSCs was shown in **Fig. 8**b. As the consequence of both improved light-harvesting efficiency and electron injection-collection efficiency at the photoanodes, the tendency of IPCE is consistent with the trend of J_{sc}. At the visible region, the significantly improved of IPCE in Au@Ag NRs incorporated DSSCs can be observed, reflecting the sensitizers around the nanorods harvesting more photons. In addition this, the IPCE of DSSCs with Au@Ag NRs show obviously broadening at longer wavelength (>600 nm) as compared with that of DSSCs with pure TiO_2. As the longitudinal plasmon absorption around 640 nm of the Au induced the light trapping, it could enhance optical density for improving photocurrent generation in this region. In general, besides the strong interaction with the dyes, the presence of the Au@Ag NRs also contributed to the long wavelength harvesting of the sunlight in the devices.

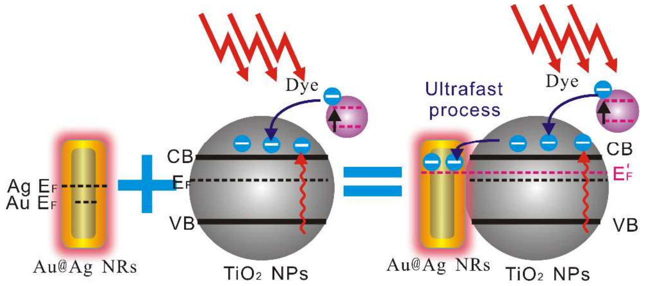

Fig. 9 Schematic illustration of the equilibration of the apparent Fermi level of the NRs /TiO_2 interface and the charge transfer-separation process.

For comparison, I-V and IPCE of DSSCs with Au@Ag NRs, Au NRs and Au NPs at the same particle concentration were discussed and shown in **Fig. S8†**. Compared to the efficiency of the reference device with 5.91%, the efficiency of devices with Au@Ag NRs, pure Au NRs and pure Au NPs are 8.43%, 7.62% and 7.51%, respectively. DSSCs with two types of NRs exhibit the enhacement IPCE over the broad spectral range than the device with pure Au NPs, and device with Au@Ag NRs has the optimal performance. DSSCs with two types of NRs exhibit the enhacement IPCE over the broad spectral range than the device with pure Au NPs, and device with Au@Ag NRs has the optimal performance. This result further clarified the broadend and strong plasmonic absorption ehnacement of the Au@Ag NRs.

2.4. Electrical properties of DSSCs

Previous discussion of absorption and I-V properties illustrated that the substantially improved of the performance was dominated by the optical aspect via SPR effect. Beyond that, the introduction of Au@Ag NRs into photoanode also impact on the charge generation, separation, and recombination process. Perhaps the electrical contribution to the final performance was relatively negligible owing to the low concentration of Au@Ag NRs. In fact, fully understanding the mechanism was benificial to develop a more effectively application of the Au@Ag NRs in the DSSCs. To further clarify the role of the Au@Ag NRs in electrondynamics process. Schematic of equilibration of the apparent Fermi level of the NRs /TiO_2 interface and the charge transfer-separation process was shown in **Fig. 9**, and detailedly discussion are as follows.

Metal nanoparticles have been known to play an important role in semiconductor-assisted photocatalytic reduction processes, and the capability to promote interfacial electron-hole transfer has been well studied.[13, 36] Previous reports indicate that the electron transfer from neighboring semiconductor to the metal nanoparticle is an ultrafast process.[34, 37] As for our experiment, the Fermi energy of both Au and Ag lies below the conduction band (CB) of TiO_2.[38] When the devices operated under illumination, photoelectrons can be generated from excited dyes and TiO_2. Due to the deep Fermi level of Ag and Au, metal NRs is capable of accepting electrons from the neigboring TiO_2/dye particles and undergoing Fermi level equilibration.[15] Considering the unique electron storage capability of the metal nanostructure,[13] electron accumulated in the metal nanorods quickly until reach the critical. After undergoing electron equilibration, the stored electrons assist in maintaining a more negative uniform Fermi level of metal/TiO_2 composite than the pristine TiO_2,[15] this process could reflect in the slightly improved open voltage of the DSSCs with Au@Ag NRs (shown in **Fig. 8**a).

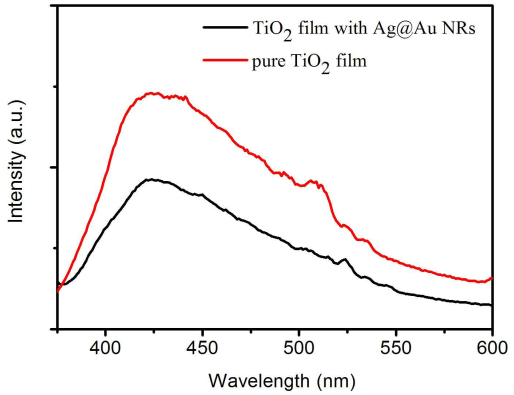

Fig. 10 Photoluminescence (PL) spectra of pure TiO_2 film, and Au@Ag NRs-modified TiO_2 film.

More than that, the uniform Fermi level at the metal/TiO_2 interface the could promote the charge transport-separation process.[35, 39] Recent studies indicate that the electron transfer from a semiconductor to a metal nanoparticle is an ultrafast process.[37] The electron storage property of metal can be beneficially used to improve the photoelectrochemical, and the noble metals such as Au and Ag could possess electron storage properties which in turn facilitates improved charge separation-transport in semiconductor/metal composite systems.[40, 41] The metal/TiO_2 interface will form electron-hole separation centers which would be beneficial in improving the movement of photo-generated electrons shuttling through the porous TiO_2 network, reducing recombination of electrons and holes, thus increasing the photocurrent.[16]

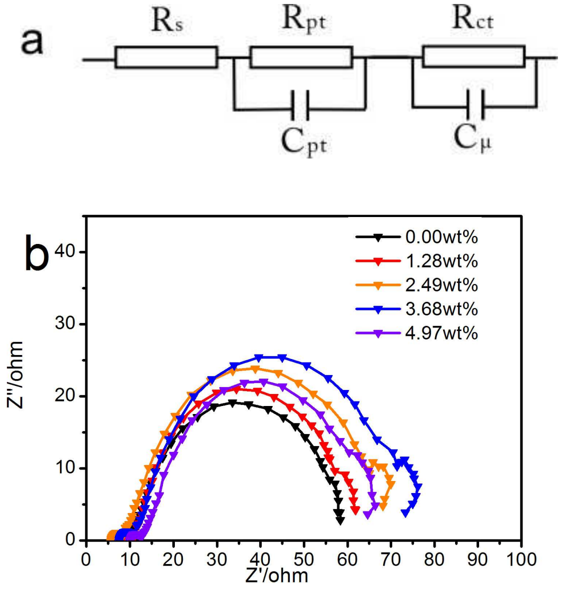

Fig. 11 Electrochemical impedance spectra of DSSCs (a) Equivalent circuit model (b) Nyquist plots of electrochemical impedance spectra of different DSSCs.

To confirm the capability of charge separation by Au@Ag NRs, the PL spectra of pure TiO_2 and Au@Ag NRs incorporated films were shown in **Fig. 10**. PL spectra were often used to study the surface processes involving electron–hole recombination of semiconductors.[42] The broad-band emission around 425 nm was assigned to the recombination of photoexcited holes with electrons occupying the singly ionized oxygen vacancies in TiO_2. The PL intensity in Au@Ag NRs incorporated film has an obvious reducing compared to pure TiO_2 film, which indicated that the recombination of electron–hole pairs in the TiO_2 film decorated with Au@Ag NRs has been suppressed effectively.

As the charge transporting-seperating process enduring at the metal/semiconductor interface was an inevitable period for operating the real device, and the difference was just the generated-photocarrier mainly from the excited dyes. Hence the PL measurement could demonstrate the capability of the charge separation by Au@Ag NRs at metal/semiconductor interface, which clarified the effect of the NRs in real DSSCs indirectly. The results of the dark-current measurement also exhibit the restraining recombination by the Au@Ag NRs.

Electrochemical impedance spectroscopy was introduced as a further proof to reveal the charge transport-recombination processes in DSSCs. With the established equivalent circuits depicted in the **Fig. 11**a, the kinetics of electrical transport and recombination can be considered in terms of a combination of the complex impedance Z_1 and Z_2.[43] The impedance spectrums of DSSCs (Nyquist plot) under dark condition were shown in **Fig. 11**b. From left to the right, the first semicircle portion (Z_1) in the Nyquist plots corresponds to the reduction reaction at the counter electrode, and the second semicircle (Z_2) was assigned to the charge recombination at the TiO_2/sensitizers/electrolyte interface. In our study, considering the introduction of metal nanostructures mainly affecting on the TiO_2/sensitizers/electrolyte interface, resistance R_{ct} (real part of Z_2) was discussed and summarized in **Table 1**.

Under dark condition, the electron process of TiO_2/sensitizers/-electrolyte interface is only the recombination between electrons and I^- / I_3^- in the electrolyte.[44] The larger the value of R_{ct} was, the slighter the electron recombination at the TiO_2/sensitizers /electrolyte interface was. Compared to the DSSC with pure TiO_2 film, R_{ct} value of the DSSCs with Au@Ag NRs increased. Larger R_{ct} reflected the lower dark current generated from charge recombination with triiodide ion at the TiO_2/dye/electrolyte interface. Here the Au@Ag NRs act as electron-hole separation centers due to the Schottky barriers at the metal/TiO_2 interface, successfully reducing charge recombination reaction. It is noted that the maximum value of R_{ct} was obtained at 3.68 wt%, and this phenomenon further demonstrated the inference that the only appropriate concentration ensured the optimal recombination-reduced ability.

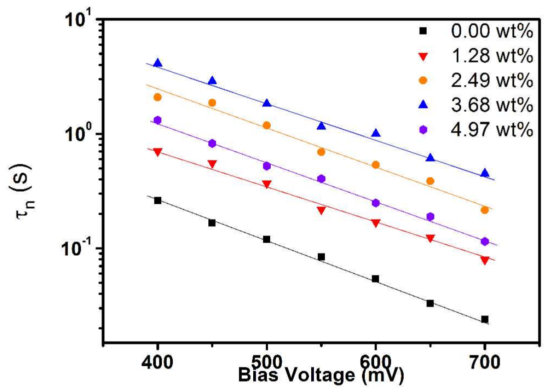

Fig. 12 Electron residence time (τ_n) in different DSSCs.

Electron residence lifetime (τ) derived from the EIS measurements with different bias voltage provided further explanation on the suppression of charge recombination in DSSCs. As is shown **in Fig. 12**, compared to the DSSCs with pure TiO_2, DSSCs with Au@Ag NRs exhibit the longer electron lifetime, revealing that the presence of the nanorods was in favour of suppressing the charge recombination. Moreover, the lifetime show an increasing-decreasing trend with the increase of the Au@Ag NRs, with the longest lifetime at 3.68 wt%, in good agreement with the dark-current and I-V curves.

Electron residence lifetime of DSSCs with different metal nanostructures was also investigated. As is shown in **Fig. S**9†, DSSCs with three nanostructures exhibit longer lifetime than the reference DSSC, which clarified that the presence of the metal nanostructures was conducive to the suppression of charge recombination. It is noted that lifetimes of three plasmonic DSSCs were little difference at the same particle concentration, cause the size of the metal nanoparticle affects the electron storage capacity. The comparison explained that the efficiency of DSSCs was mainly influenced by the plasmonic absorption enhancement property, which precisely is the unique advantage of the Au@Ag NRs.

3. Conclusion

In this article, a unique core-shell Au@Ag NRs is prepared and applied in DSSCs. It is found that the use of plasmonic nanorods significantly improved the performance of DSSCs. By efficiently affecting on the sensitizers and converting low energy sunlight into electricity, an optimal performance of device with nanords reach up to 8.43% can be obtained, which was almost 40% higher than the device without Au@Ag NRs. Considering the optical property of the nanorods can be tuned via the aspect ratio, beyond the development of strong plasmonic absorption at visible region, effective light harvesting at longer wavelengths is expected to be achieved via regulating the ratio. This plasmonic approach has the huge potential to act as the assistance and supplement to various universal sensitizers for higher LHE, and further research is needed to utilize the novel prospects on various areas. In general, we hope that our study could provide new ways to develop applications on organic sola cells, CIGS thin film solar cells and perovskite solar cells.

Experimental Section

Synthesis of (Au core)−(Ag shell) nanorods, Au nanorods and Au nanoparticles

AuNRs were synthesized via a seed mediated method reported by Murphy et al.[45] For control of the thickness of Ag shell, different concentration of $AgNO_3$ and ascorbic acid lead to the sized-tunable (Au core)-(Ag shell) nanorods.[25] The as-synthesized Au NRs solution was centrifuged at 10000 rpm for 60 min, then redispersed into aqueous CTAC solutions (0.08 M) at the same volume. 0.45 mL $AgNO_3$ (0.008 M) were subsequently added into the 2 mL Au nanorod solution, followed by the addition of 0.015 mL ascorbic acid solutions (0.1 M). The resultant solutions were kept in an isothermal oven at 60 °C for 4 h. Then the bare (Au core)−(Ag shell) nanorods were obtained.

The initial Au@Ag NRs were dispersed into deionized water and centrifuged at 10000 rpm, and this process was repeated several times for removing the residual CTAC, then the 0.1g precipitate was added into 30 mL deionized water. 0.012 g titanium tetraisopropoxide (TTIP) as the TiO_2 precursor was added in the solution, and stirring was continued for an additional 30 min at 60 °C to ensure completion of the reaction. Au@Ag NRs with thin TiO_2 shell layer were then obtained. The solution was washed several times and centrifuged at 6000 rpm to remove TTIP. The final precipitation was air dried and doped in pure TiO_2 paste with various ratios.

Here the **ratio** between TTIP and Au@Ag NRs mainly determined the thickness of the TiO_2, and the dispersion and washing process influenced the integrity of the coating.

Pure Au nanorods were also synthesized via a seed mediated method reported by Murphy et al. Pure Au nanoparticles were synthesized via the Liz-Marzan et al.[46] The TiO_2 coating process is similar to the TiO_2 coated Au@Ag NRs.

Fabrication of photoanodes and DSSCs

Glass substrates coated FTO (Nippon Sheet Glass, Japan, 2.2 mm thickness, 14 Ω □$^{-1}$) were cleaned in a detergent solution for 30 min in an ultrasonic bath, rinsed with deionized water, isopropanol and EtOH for 30 min successively. The pure TiO_2 pastes were prepared by TiO_2 powder (Degussa, P25), different photoanodes were synthesized by stiring various amounts of treated Au@Ag NRs into the pure TiO_2 pastes according to a series of mass ratios (Au@Ag NRs:P25=0.00%, 1.28%, 2.49%, 3.68%, 4.97%), (Au NRs:P25=5.44%), (Au NPs:P25=4.74%). Then the seven kinds of transparent TiO_2 pastes were screen-printed onto the FTO as the transparent layer，then the coated films were dried at temperature of 125 °C for 6 min. This screen-printing procedure with the paste was repeated to obtain an appropriate thickness of 8 μm of TiO_2 for the working electrode. The coated substrates were thermally treated under an air flow at 325 °C for 5 min, 375 °C for 10 min, 450 °C for 15 min and 500 °C for 15 min, respectively. After cooling down to 80 °C, the TiO_2 electrode was stained by immersing it into a dye solution containing N719 sensitizer (300 μm) in a mixture of acetonitrile and tert-butyl alcohol (volume ratio: 1:1) overnight. The TiO_2 photoanodes adsorbed dye and 2 nm Pt counter electrodes were assembled into a sealed sandwich-type cell by a 60 µm hot-melt ionomer film Bynel (Dupont) as a spacer between the electrodes. A drop of the electrolyte solution, 0.6 M 1-butyl-3-methyl imidazolium iodide (BMII), 0.03 MI_2, 0.02 M LiI, 0.10 M guanidinium thiocyanate and 0.5 M 4-tert-butylpyridine in a mixture of acetonitrile and valeronitrile (volume ratio, 85:15), was injected into the cell.

Characterization

The morphology of the Au@Ag NRs was investigated by scanning electron microscopy (SEM) (Quanta 250, FEI) and transmission electron microscope (TEM) (2100, JEOL). The chemical species of the Au@Ag NRs were analyzed by Energy-dispersive X-ray spectroscopy (EDX) (EDAX, Quanta 250, FEI) The crystalline structure of the various TiO_2 films was determined by X-ray diffraction (XRD) (D/MAX-2400, Rigaku, Japan). The UV-vis absorption spectra of the Au@Ag NRs were obtained on a UV-vis spectrophotometer (Fluoromax 4, HORIBA Jobin Yvon, USA). The Incident Photon-to-current Conversion Efficiency (IPCE) was evaluated by the solar cell quantum efficiency measurement system (SolarCellScan 100, Zolix instruments. Co. Ltd). The photocurrent density-voltage characteristics were evaluated by a AAA solar simulator (XES-301S, SAN-EI Electric. Co. Ltd.), AM 1.5G illumination (100 mW cm^{-2} in intensity), and a Keithley digital source meter (Model 2602). Electrochemical impedance spectra (EIS) of the cells were evaluated using CHI-660D over the frequency range of 0.1 Hz~100 KHz under the conditions of open circuit under 100 mW cm^{-2}. All the cells have an active area about 0.25 cm^2.

Acknowledgements

This work was financially supported by Basic Research Program of China (2013CB328705), National Natural Science Foundation of China (Grant Nos. 61275034, 61106123), Ph.D. Programs Foundation of Ministry of Education of China (Grant No. 20130201110065); Fundamental Research Funds for the Central Universities (Grant No. xjj2012087). The SEM work was done at International Center for Dielectric Research (ICDR)，Xi'an Jiaotong University，Xi'an,China; The authors also thank Ms. Dai for her help in using SEM.

Notes and references

[a] Key Laboratory of Photonics Technology for information, Key Laboratory for Physical Electronics and Devices of the Ministry of Education, School of Electronic and Information Engineering, Xi'an Jiaotong University, Xi'an 710049, P. R. China
Tel: +86-29-82664867
E-mail: zhaoxinwu@mail.xjtu.edu.cn

[b] Polymer and Color Chemistry Program, University of North Carolina, NC 27695, USA, ahmed_el-shafei@ncsu.edu

1. B. Oregan and M. Gratzel, *Nature*, 1991, **353**, 737-740.
2. S. Mathew, A. Yella, P. Gao, R. Humphry-Baker, B. F. E. Curchod, N. Ashari-Astani, I. Tavernelli, U. Rothlisberger, M. K. Nazeeruddin and M. Gratzel, *Nature Chemistry*, 2014, **6**, 242-247.
3. B. E. Hardin, H. J. Snaith and M. D. McGehee, *Nature Photonics*, 2012, **6**, 162-169.
4. M. Gratzel, *Nature*, 2001, **414**, 338-344.
5. A. Yella, H. W. Lee, H. N. Tsao, C. Y. Yi, A. K. Chandiran, M. K. Nazeeruddin, E. W. G. Diau, C. Y. Yeh, S. M. Zakeeruddin and M. Gratzel, *Science*, 2011, **334**, 629-634.
6. T. W. Hamann, R. A. Jensen, A. B. F. Martinson, H. Van Ryswyk and J. T. Hupp, *Energy & Environmental Science*, 2008, **1**, 66-78.
7. Y. M. Cao, Y. Bai, Q. J. Yu, Y. M. Cheng, S. Liu, D. Shi, F. F. Gao and P. Wang, *J. Phys. Chem. C*, 2009, **113**, 6290-6297.
8. Z. S. Wang, Y. Cui, K. Hara, Y. Dan-Oh, C. Kasada and A. Shinpo, *Adv. Mater.*, 2007, **19**, 1138-1141.
9. J. H. Yum, P. Walter, S. Huber, D. Rentsch, T. Geiger, F. Nuesch, F. De Angelis, M. Gratzel and M. K. Nazeeruddin, *J. Am. Chem. Soc.*, 2007, **129**, 10320-+.
10. P. Y. Reddy, L. Giribabu, C. Lyness, H. J. Snaith, C. Vijaykumar, M. Chandrasekharam, M. Lakshmikantam, J. H. Yum, K. Kalyanasundaram, M. Graetzel and M. K. Nazeeruddin, *Angew. Chem. Int. Edit.*, 2007, **46**, 373-376.
11. Q. Q. Miao, L. Q. Wu, J. N. Cui, M. D. Huang and T. L. Ma, *Adv. Mater.*, 2011, **23**, 2764-2768.
12. G. K. Mor, J. Basham, M. Paulose, S. Kim, O. K. Varghese, A. Vaish, S. Yoriya and C. A. Grimes, *Nano Letters*, 2010, **10**, 2387-2394.
13. A. Takai and P. V. Kamat, *Acs Nano*, 2011, **5**, 7369-7376.
14. H. Dong, Z. X. Wu, Y. C. Gao, A. El-Shafei, B. Jiao, Y. Dai and X. Hou, *Org. Electron.*, 2014, **15**, 1641-1649.
15. H. Choi, W. T. Chen and P. V. Kamat, *Acs Nano*, 2012, **6**, 4418-4427.
16. K. M. Guo, M. Y. Li, X. L. Fang, X. L. Liu, B. Sebo, Y. D. Zhu, Z. Q. Hu and X. Z. Zhao, *J. Power Sources*, 2013, **230**, 155-160.
17. Y. Li, H. Wang, Q. Y. Feng, G. Zhou and Z. S. Wang, *Energy & Environmental Science*, 2013, **6**, 2156-2165.
18. Z. B. Tian, L. Q. Wang, L. S. Jia, Q. B. Li, Q. Q. Song, S. Su and H. Yang, *Rsc Advances*, 2013, **3**, 6369-6376.
19. M. D. Brown, T. Suteewong, R. S. S. Kumar, V. D'Innocenzo, A. Petrozza, M. M. Lee, U. Wiesner and H. J. Snaith, *Nano Letters*, 2011, **11**, 438-445.
20. X. N. Dang, J. F. Qi, M. T. Klug, P. Y. Chen, D. S. Yun, N. X. Fang, P. T. Hammond and A. M. Belcher, *Nano Letters*, 2013, **13**, 637-642.
21. S. D. Standridge, G. C. Schatz and J. T. Hupp, *J. Am. Chem. Soc.*, 2009, **131**, 8407-+.
22. H. Dong, Z. X. Wu, Y. C. Gao, A. El-Shafei, S. Y. Ning, J. Xi, B. Jiao and X. Hou, *Org. Electron.*, 2014, **15**, 2847-2854.

23. F. L. Su, T. Wang, R. Lv, J. J. Zhang, P. Zhang, J. W. Lu and J. L. Gong, *Nanoscale*, 2013, **5**, 9001-9009.
24. S. Muduli, O. Game, V. Dhas, K. Vijayamohanan, K. A. Bogle, N. Valanoor and S. B. Ogale, *Sol. Energy*, 2012, **86**, 1428-1434.
25. R. B. Jiang, H. J. Chen, L. Shao, Q. Li and J. F. Wang, *Adv. Mater.*, 2012, **24**, Op200-Op207.
26. B. Pietrobon, M. McEachran and V. Kitaev, *Acs Nano*, 2009, **3**, 21-26.
27. W. Ni, X. Kou, Z. Yang and J. F. Wang, *Acs Nano*, 2008, **2**, 677-686.
28. Z. S. Yang and H. T. Chang, *Nanotechnology*, 2006, **17**, 2304-2310.
29. Y. U. Xiang, X. C. Wu, D. F. Liu, Z. Y. Li, W. G. Chu, L. L. Feng, K. Zhang, W. Y. Zhou and S. S. Xie, *Langmuir.*, 2008, **24**, 3465-3470.
30. Y. Okuno, K. Nishioka, A. Kiya, N. Nakashima, A. Ishibashi and Y. Niidome, *Nanoscale*, 2010, **2**, 1489-1493.
31. N. J. Borys, M. J. Walter and J. M. Lupton, *Phys. Rev. B*, 2009, **80**.
32. K. M. Guo, M. Y. Li, X. L. Fang, X. L. Liu, Y. D. Zhu, Z. Q. Hu and X. Z. Zhao, *Journal of Materials Chemistry A*, 2013, **1**, 7229-7234.
33. S. Chang, Q. Li, X. D. Xiao, K. Y. Wong and T. Chen, *Energy & Environmental Science*, 2012, **5**, 9444-9448.
34. C. Harris and P. V. Kamat, *Acs Nano*, 2010, **4**, 7321-7330.
35. R. A. Naphade, M. Tathavadekar, J. P. Jog, S. Agarkar and S. Ogale, *Journal of Materials Chemistry A*, 2014, **2**, 975-984.
36. P. V. Kamat, *Journal of Physical Chemistry Letters*, 2012, **3**, 663-672.
37. R. Katoh, A. Furube, K. Yamanaka and T. Morikawa, *Journal of Physical Chemistry Letters*, 2010, **1**, 3261-3265.
38. M. Jakob, H. Levanon and P. V. Kamat, *Nano Letters*, 2003, **3**, 353-358.
39. Y. Y. Lou, S. Yuan, Y. Zhao, P. F. Hu, Z. Y. Wang, M. H. Zhang, L. Y. Shi and D. D. Li, *Dalton Transactions*, 2013, **42**, 5330-5337.
40. P. V. Kamat and B. Shanghavi, *J. Phys. Chem. B*, 1997, **101**, 7675-7679.
41. G. Merga, L. C. Cass, D. M. Chipman and D. Meisel, *J. Am. Chem. Soc.*, 2008, **130**, 7067-7076.
42. M. D. Ye, D. J. Zheng, M. Q. Lv, C. Chen, C. J. Lin and Z. Q. Lin, *Adv. Mater.*, 2013, **25**, 3039-3044.
43. L. Y. Han, N. Koide, Y. Chiba and T. Mitate, *Appl. Phys. Lett.*, 2004, **84**, 2433-2435.
44. R. Gao, G. D. Niu, L. D. Wang, B. B. Ma and Y. Qiu, *Acta Phys-chim. Sin.*, 2013, **29**, 73-81.
45. N. R. Jana, L. Gearheart and C. J. Murphy, *Adv. Mater.*, 2001, **13**, 1389-1393.
46. J. Rodriguez-Fernandez, J. Perez-Juste, F. J. G. de Abajo and L. M. Liz-Marzan, *Langmuir.*, 2006, **22**, 7007-7010.

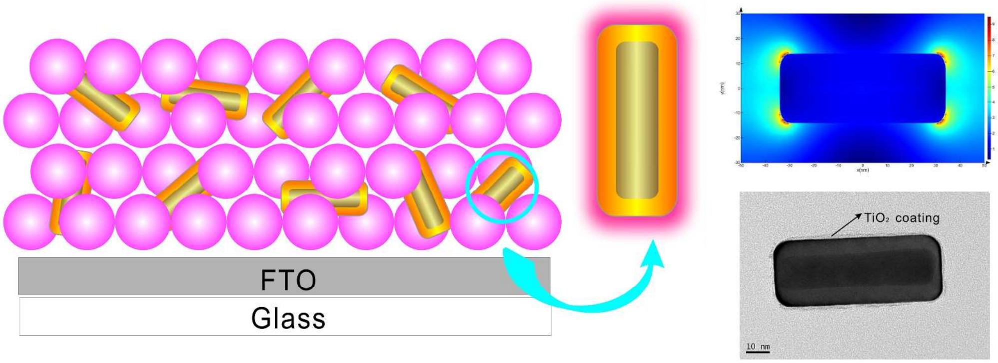

340x130mm (300 x 300 DPI)